

A study on the effect of pore and particle distributions on the soil water characteristic curve of compacted loess

Yu Wang (✉ faithwang2018@chd.edu.cn)

Department of Geological Engineering, Chang'an University

Tonglu Li (✉ dcdgx08@chd.edu.cn)

Chang'an University <https://orcid.org/0000-0001-6561-1871>

Chenxi Zhao

Chang'an University

Xiaokun Hou

Institute of Geophysics: Institute of Geology and Geophysics Chinese Academy of Sciences

Ping Li

Chang'an University

Yaguo Zhang

Chang'an University

Research Article

Keywords: soil water characteristics, compacted loess soil, pore, particle, filter paper method, MIP, SEM

Posted Date: June 12th, 2021

DOI: <https://doi.org/10.21203/rs.3.rs-167139/v1>

License: © ⓘ This work is licensed under a Creative Commons Attribution 4.0 International License.

[Read Full License](#)

Version of Record: A version of this preprint was published at Environmental Earth Sciences on November 1st, 2021. See the published version at <https://doi.org/10.1007/s12665-021-09973-0>.

Abstract

Compacted loess soil is used as a geo-material in many engineering projects such as building foundations and highway embankments. Water infiltration characteristics and post settlement of the compacted loess in large construction projects of Northwest China have received increasing attention from researchers and investors. These behaviors are closely related to the soil water characteristics. This study aims to investigate the soil water characteristic curves (SWCCs) of compacted loess soil with different dry densities and to reveal the responsible micro-mechanisms for soil water characteristics. Loess soil collected from the new district of Yan'an City, China, is prepared into five dry density groups. The SWCC of each group in the suction range of 0–100,000 kPa is measured using the filter paper method (FPM). Two-dimensional (2D) images and the pore size distribution (PSD) curves of the specimens are tested by scanning electron microscopy (SEM) and the mercury pressure method (MIP), respectively. The results of this study highlight that the compaction behavior mainly influences the pores with a radius (r) in the range of 1–10 μm , and has no influence on the pores of $r < 0.5 \mu\text{m}$. The particle shapes among the five dry densities groups are similar. The characteristics of the PSD curves of the compacted loess soil correspond well to the SWCCs. The suction of the SWCCs increases with increasing dry density in the lower suction range of 0–100 kPa. In contrast, suction among the five dry density groups is almost identical in the suction range exceeding 100 kPa. The results of the study are helpful to understand the SWCC and microstructure characteristics of compacted loess with different dry densities.

Introduction

There has been a rapid expansion of a modern city in the Chinese Loess Plateau for nearly a decade, which has involved the flattening of hills and filling in gullies to form flat land that is suitable for the construction of urban or industrial infrastructure (Li et al., 2014). Studies into the filled loess in the new district of the city of Yan'an, China (Fig.1) have shown that the dry density of the compacted loess is highly variable. The filling of unsaturated soil may be in a complex hydraulic state through surface water infiltration and groundwater penetration. These changes might result in a large amount of post-filling ground settlement that may persist for an extended period. The soil water characteristic curve (SWCC) is essential to predict the after-filling settlement of the filled ground. Therefore, the current study aimed to investigate the characteristics of SWCCs for compacted loess material of different dry densities and to identify the micro-structural reasons for the differences.

The SWCC describes the state of the energy balance between soil and water, which is expressed as the relationship between matrix suction and water content (gravimetric, volumetric, or saturation) (Lu 2019). The SWCC is a fundamental property of unsaturated soil and plays a crucial role in understanding and modeling the changes in shear strength, permeability, and volume change of unsaturated soils (Vanapalli et al. 2001; Ning and Likos 2004; Fredlund and Delwyn 2006; Lu and Likos 2006; Rahardjo and Leong 2006). The methods used to measure matric suction include the tensiometer method, axial translation technology, and the filter paper method. Among these methods, the filter paper method (FPM) can be used to measure suction up to a maximum of 300,000 kPa (Pincus et al. 1994), and is considered to be a

simple method with no impact on the soil structure under atmospheric pressure. The principle of FPM can be understood as the transport of pore water in the soil to wet or dry the filter paper. Under this method, the matric suction is measured as the contact between the soil specimen and the filter paper, whereas total suction is calculated as the sum of matric suction and osmotic suction since there is no direct contact between total suction and the filter paper (Al-Khafaf and Hanks 1974; Lu and Likos 2006).

The effect of dry density (also known as the void ratio or compactness) on SWCC has been a focus of previous studies (Zhou et al. 2012; Eyo et al. 2020). It is generally accepted that soil with a higher compactness will show higher suction at the same water content (Vanapalli et al. 1999; Birle et al. 2008). SWCCs for different soil dry densities will intersect at a critical suction point, beyond which they will diverge. Within the range of suction below the critical point, the curve of the SWCC for small dry density will be positioned above that of large dry density, with the opposite true for suction beyond the critical point (Jiang et al. 2017). However, these characteristics are observed under the suction-volume water content coordinate. Under the suction-gravimetric water content coordinates (mass of water content = volume of water content / dry density), the position of the intersection point will shift back and the curves after the intersection point will tend to converge. Hou et al. (2020) and Salager et al. (2013) observed the phenomenon using the gravimetric water content. However, there has not been sufficient attention paid to this regular pattern, with related discussion in some studies (Miguel and Bonder 2012; Ran et al. 2013; Bharat and Gopak 2020). It is worth noting that some scholars have concluded that there is no difference in the behaviors of different SWCCs under a large suction level (Birle 2012; Zhang et al. 2017). Based on this rule, the mathematical expression of matrix suction can be divided into two parts, namely two-dimensional and one-dimensional matrix suction (Baker and Frydman 2009). In contrast, most expressions of the SWCC were two-dimensional equations of suction that change with changing water content (Mbonimpa et al. 2006; Zhou et al. 2012; Li et al. 2020). Therefore, the effect of dry density on SWCC is a subject worthy of attention. There is a need to conduct a series of SWCC experiments to clarify the changes in SWCCs of compacted soil under different dry densities.

Soil mineral composition, particle size gradation, density, pore structure and organic matter are all factors influencing the SWCC (Mijares and Khire 2010; Della et al. 2011; Jiang et al. 2017). The pore structure of soil within a certain range of pore size can play a decisive role in the characteristics of the SWCC (Romero et al. 1999). Within the investigation of soil structures, mercury intrusion porosimeter (MIP) is usually used to identify the pore size distribution and scanning electron microscopy (SEM) is used for identifying the geometric characteristics of pores and particles (Jiang et al. 2014, 2019). In particular, two-dimensional (2D) images captured by scanning electron microscopy (SEM) allow a cross-sectional visual examination of the morphological distribution of pores and particles (Li and Li 2017, 2019). Many studies have used MIP to investigate the relationship between pore size distribution and changes to water volume or the water permeability of unsaturated soils (Sasanian and Newson 2013; Wang et al. 2019). Images of soil microstructure have also been utilized to explain the mechanisms of soil macroscopic behaviors, such as hydraulic conductivity, compressibility, shrinkage, and expansion (Delage et al. 1996; Nie et al. 2015; Li et al. 2018). These studies have illustrated the importance of the size, shape, and arrangement of soil particles and the distribution of pores for explaining soil-water behavior. A series of soil

microstructure experiments are required to explore the effect of particles and pores on the dry density and SWCC of compacted soil so as to clarify how SWCCs change under different soil dry densities.

The present study investigated the soil in the filled-in area by collecting soil from the area and preparing compacted specimens of five different dry densities using the static pressure method. The SWCCs of the specimens were analyzed using a modified FPM method in the range of 10–10⁵ kPa. MIP tests and 2D-SEM observation were conducted to obtain further insight into the micro-scale characteristics of SWCCs for specimens of different dry densities. The results of this study is helpful to deepen our understanding of the SWCC behavior with different dry densities and can be used to analyze the hydraulic conditions of the filling area in future.

Study Area And Materials

The study area of the present study is the new district of Yan'an city, central China. The original topography of the area was characteristic of hilly natural loess. However, this area has been flattened through the cutting of hills and filling in of gullies. The first stage of the project has already been completed and some of the infrastructure has been constructed. Areas in which hills were cut have naturally over-consolidated soil, providing a good foundation. However, the artificially filled area was formed by layered rolling, resulting in spatial variability in the dry densities of the compacted soil layer with a thickness of ~100 m. As shown in Fig. 2, the results of laboratory tests of 19 boreholes in the filled soil area indicate a normal distribution of the dry densities of the compacted loess specimens, mostly in the range of 1.40–1.80 g/cm⁻³, accounting for 97% of the total. These results suggest that the dry densities of much of the area fall far below the maximum value of ~1.8 g/cm⁻³ according to the laboratory standard compaction test result and much lower than required standard dry density of ~1.7 g/cm⁻³. This indicates the challenge presented by infilling at such a large scale and high speed for compacting the soil to the preferred water content and designed compression ratio.

Loess soil was collected from the filled area with a liquid limit and plastic limit of 28.5% and 18.7%, respectively. The soil contents of clay minerals and quartz were 22.6% and 44.6%, respectively. As shown in Fig. 3, the particle size distribution of the soil was analyzed using the Bettersize-2000 Laser Analyzer. Silt (0.002–0.05 mm) and clay (< 0.002 mm) particles comprised 65.96% and 6.55% of the total soil particles, respectively. Therefore, the soil could be classified as silty clay according to the Unified Soil Classification System (International 2006). Five groups of compacted specimens with different dry densities were remolded using the static compaction method and the average water content of the surface layer (10%) was used as the initial molding water content. Each group of specimens had the same dry density, and the five densities of the specimens were 1.40 g/cm⁻³, 1.50 g/cm⁻³, 1.60 g/cm⁻³, 1.70 g/cm⁻³, and 1.80 g/cm⁻³. Table 1 lists the physical parameters of the compacted specimens. Specimens with a dry density measurement error exceeding ± 0.01 g/cm⁻³ were discarded to ensure the uniformity of each group of specimens.

Laboratory test

Measurement of the SWCC

SWCC of the compacted specimens was measured by FPM, as shown in Fig. 4. Before testing, test filter paper (Whatman No.42) and ordinary filter paper used in the study were sterilized by soaking in formalin solution (2%) and dried in an oven at a temperature of 105 °C for 4 h (ASTM, 2011), following which they were stored in a desiccant for later use. The diameter of the test filter paper of 42.5 mm was slightly smaller than the diameter of the specimens. The ordinary filter paper was cut to same area as the surface area of the specimen (diameter of 61.8 mm) and was used to cover the surfaces of specimens to prevent falling slag and contamination of the test filter paper. The experiment mainly includes the following four steps:

(A) All the soil specimens were dried first, then they were re-hydrated to different degree of water contents using the water content interval of 1% or 2% , from very dry to saturated conditions respectively. Each water content has two parallel specimens, with each water content requiring two specimens.

(B) Two soil specimens with the same water content were vertically stacked with a section of Whatman No.42 filter paper placed between them.

(C) The specific processes used to create a simple sealing environment were: (1) the gap in the middle of the two specimens was tightly fixed using waterproof tape; (2) the entire specimen was wrapped with plastic film; (3) the specimen was then wrapped with aluminum foil; (4) the aluminum foil was brushed with melted paraffin wax.

(D) The specimens were rapidly unwrapped and weighed after being placed in an incubator (20 °C) for at least 15 days. Both the wet and dry weights of the specimens and Whatman No.42 filter paper were weighed using a balance with different accuracies.

Using the processes described above, the water contents of the test filter paper and the specimens were calculated. The matric suction values of the specimens were calculated using the calibration method shown in Eq. (1) (ASTM 2011). As an example, Fig. 5 plots soil water content against matric suction of the No.2 specimen (hollow circles). The experimental results of the pressure plate method are also plotted in Fig. 5 (black squares) in the lower suction range, which indicates a good agreement between the data of the two methods in the overlap range. Therefore, it can be concluded that FPM was reliable for measuring the SWCCs of these compacted soils.

$$\begin{aligned}\log_{10}\psi &= 5.327 - 0.0779 \times w_{fp} \quad (w_{fp} < 45.26\%) \\ \log_{10}\psi &= 2.412 - 0.0135 \times w_{fp} \quad (w_{fp} > 45.26\%) \end{aligned} \tag{1}$$

In Eq. (1), ψ represents matrix suction (kPa) and w_{cfp} represents the change in the gravity water content of the filter paper (%).

Measurement of microstructure

The present study used two methods to observe the soil microstructure, namely two-dimensional scanning electron microscopy (2D-SEM) and mercury intrusion porosimetry (MIP). Image-Pro Plus 6.0 (IPP 6.0) software was used to process the photos obtained by 2D-SEM.

The processing of the soil sample for analysis through the 2D-SEM method in the current study mainly included drying, impregnation with epoxy resin, cutting, rough grinding, and polishing (Li and Li 2017, 2019). 2D-SEM allowed the visualization of the morphological distribution of pores and particles on the cross-sectional surface of a sample. It is worth noting that drying the sample may have an impact on soil microstructure, such as pores and aggregates. Oven drying method can result in pore and aggregates shrinkage (Zhang et al. 2011). Freeze drying is rapid and generally regarded to minimize the change of soil microstructure (Deacon et al. 2008). Therefore, the freeze-drying method was used in the current study.

The present study used the IPP 6.0 software to visualize the pore structures of samples (Xu et al. 2020), and pore diameter, particle circularity, convexity and elongation were selected for analysis. The use of the software mainly includes the following four steps: (1) establishing the same scale as that to which the image has been magnified; (2) using contrast enhancement, denoising, filtering, and other tools to clarify the boundary between pores and particles; (3) using the segmentation tool to mask the particles and pores with white and black colors, respectively; (4) using counting tools to enumerate the parameters of pores or particles.

MIP is based on the phenomenon of capillarity and is used to quantitatively analyze the microstructure of compacted soil (Delage et al. 1996; Romero et al. 1999; Sasanian and Newson 2013). This method mainly includes the following four steps: (1) cutting the specimen into a cylinder shape with about 1 cm in diameter and 1.5 cm in height, then freeze-drying; (2) weighing the sample and the penetrometer and then entering the relevant parameters into the software; (3) placing the cylinder sample in the calibrated penetrometer and sequentially conducting low-pressure and high-pressure analysis; (4) safe disposal of the samples after the removal of mercury. The present study measured the amount of mercury in the pores of the five specimens under external pressures between 0 and 400 MPa using the Autopore-9500 instrument.

Experimental Results

Soil water characteristics

The present study fits the SWCC test data using the Van Genuchten (1980) equation, namely Eq. (2). This model is widely used for various dry densities, and the use of parameter w_r ensures that the knee point of higher suction approaches to residual water content. Parameter a is related to the air entry value of soil, n is the inflection rate in the transient zone, which reflects the uniformity of the pore size distribution. Table 2 lists the fitting parameters of the model and Fig. 6 shows the fitting curves.

$$w_w = w_r + \frac{w_s - w_r}{[1 + (a\psi)^n]^m} \quad (2)$$

In Eq. (2), w_s is the gravimetric water content (%), w_s is the saturated gravimetric water content (%), w_r is the residual gravimetric water content (%; $w_r \sim 10\%$), and ψ is the matric suction (kPa; $e \sim 2.718$).

As shown in Fig. 6, the SWCCs can be divided into three stages (Vanapalli et al. 1999): (1) the boundary effect stage; (2) the transient stage and; (3) the residual stage. The soil will experience from the residual stage to the transient stage, and finally to the boundary stage during the wetting process. The air occlusion value (AOV) is widely used to demarcate the boundary stage and the transition corresponding to the air entry value (AEV) (Della et al. 2011), and can be determined using the method proposed by Vanapalli et al. (1999).

Fig. 6 shows that the water content of the soil increases gradually at the start of the wetting process (residual stage). The SWCCs of the specimens with different densities are almost identical in the residual stage with the water content less than 10%. Rapid increase occurs during the transition stage, which is strongly associated with dry density. Furthermore, with the increase of the dry density, the saturated water content decreases from 34.5% to 18.7%, whereas the AOV increases from 8 kPa to 25 kPa, resulting in a wider suction range in the boundary zone and a narrower range in the transition zone, while the residual suction is the same for the five SWCCs. Figure 6 also conveys an important message that the intersection of the five curves appear to be near 100 kPa and that the water content of the soil specimen is close to 10%. Therefore, the five curves can be piecewise fitted, with the van Genuchten (1980) and linear fitting models used in the case of suction being less than and exceeding 100 kPa, respectively.

The equi-suction lines in Fig. 7 shows that lines for suction below 100 kPa have a varied degree of inclination. When equi-suction line is less than 8 kPa (corresponding to the minimum AOV), the water content of specimens with lower dry density is higher, otherwise the water content is lower. However, lines for suction exceeding 100 kPa are approximately vertical, which means that the dry density or pore ratio of the compacted soil in the high suction phase is not correlated with the change in suction. As argued by Delage (2007) and Bake (2009), there is no correlation between the change in suction and the dry density or pore ratio of the soil in high suction ranges.

Observations of soil microstructure

Particles and pores

Fig. 8(a) shows 2D images of the soil specimens with dry densities of 1.40 g/cm^{-3} (No. 1), 1.60 g/cm^{-3} (No. 3), and 1.80 g/cm^{-3} (No. 5) captured using SEM at a magnification of $\times 1,000$. The compacted soil is an assemblage of particles and aggregations (Della et al. 2011), and the particles can be subdivided into sand ($> 60 \mu\text{m}$), silt ($2-60 \mu\text{m}$), and clay ($< 2 \mu\text{m}$). Within the captured 2D-SEM images at $\times 1,000$ magnification, clay particles have a radius of less than $1 \mu\text{m}$ and are hard to identify, whereas silt and

sand particles can be clearly observed. It can be seen from Fig. 8(a) that for specimens with the same soil properties and molding water content, the total area of particles increases with increasing dry density, the contact between particles changes from point-to-point contact to surface contact, and the number of aggregates or coagulum gradually increases.

The shape of particles is often described using three parameters (Pagliai et al. 2004; Altuhafi et al. 2016): (1) circularity; (2) convexity and, (3) elongation. Circularity is a measure of particle roundness, which is equal to " $4\pi\text{Area}/\text{Perimeter}^2$ ". Elongation measures the difference between the major axis and the minor axis of a particle and is expressed as " $1 - \text{aspect ratio}$ " (aspect ratio = minor axis/major axis). Convexity is a parameter describing the surface roughness of particles and is given by the ratio of the "convex hull perimeter" (Li 2013). The texture and shape of particles can be described as increasingly smooth and round as the values of these three parameters move closer to 1. The results of the present study indicate no obvious concentrated distribution in the circularity of particles in each specimen, with elongation in the range of 0.5–0.8 and convexity mostly exceeding 0.90 [Fig. 8 (b)]. Therefore, the particle shape distributions of specimens with different dry densities are similar.

The processing of 2D-SEM images by IPP 6.0 allows the pore elements to be separately identified and rendered. As shown in Fig. 9 and consistent with the pore size classification by Lei (1987) and Gao (1980, 1981), the current study classifies pores exceeding 1 μm and 16 μm as intra-granular pores (falling within the micro-pore category) and overhead pores (falling within the macro-pore category), respectively, whereas pores with pore sizes falling between these classifications are classified as inter-granular pores (falling within the mesopore category). Overhead pores are formed by a loose accumulation of skeleton particles. Inter-granular pores are formed by the mosaic and arrangement of particles in three-dimensional space, and arrangement in a crisscross pattern on the two-dimensional plane. Intra-granular pores are formed in inside the aggregates or coagulum, and regardless of the skeleton arrangement. It can be observed from the Fig. 9 that an increase in dry density results in a reduction of overhead pores (green area) and an increase in inter-granular pores (blue area). There is no comparison and discussion on micropores since they cannot be accurately identified in the current study.

Pore size distribution curves

As shown in Fig. 10, the pore size distribution (PSD) curves of the five specimens are measured by MIP to quantitatively investigate the pore characteristics of specimens with different dry densities. In the current study, the definition of dominant pore size (DPS) is the pore radius corresponding to the peak of PSD curve, the definition of the upper limit pore size (ULPS) is the pore radius corresponding to the marked change when the slope changed from gentle to steep (Fig. 10). Of note is that the pore radii of all specimens are within the range of 0.01–100 μm , with the differences between specimens mainly reflect in the size and number of dominant pores, whereas there are slight differences among the specimens in terms of the radii less than 0.5 μm .

As shown in Fig. 11, the differences in DPS and ULPS decrease rapidly and tend to stabilize. Both the DPS and ULPS of No. 1 are the largest, whereas those of No. 4 and No. 5 are the smallest. Moreover, the DPS and ULPS of compacted loess tend to be of the same size (~ 2 and $3 \mu\text{m}$ respectively) with a decrease in dry density to 1.70 g/cm^{-3} . Therefore, it can be considered that the differences in pore size were mainly due to the number of pores rather than the size of pores as the dry density increased above 1.70 g/cm^{-3} .

Discussion

Effect of particle characteristics on the SWCC

The number of particles and aggregates in a unit volume can narrow the channel of water storage, which points to a negative correlation between water holding capacity and dry density. So the saturated water content decreases with increasing dry density. In addition, the particle shape distributions (including circularity, convexity and elongation) of all the specimens with different dry density are almost similar [Fig. 8(b)]. Thereby, the particle shape may not contribute to the difference of specimens with different dry densities.

Effect of the pore characteristics on the SWCC

After converting the pore radius into suction using the Yang-Laplace equation (Eq. 3) (Washburn 1921; Diamond 1970), the PSDs and SWCCs are plotted on the same coordinates for comparison to further study the influence of pore size on soil water characteristics.

$$u_a - u_w = \frac{2T_s \cos \alpha}{r} \quad (3)$$

In Eq. (3), $u_a - u_w$ is the suction (kPa), T_s is surface tension of water (72.75 mN/m), α is the contact angle between soil and water ($^\circ$), and r is the radius of the pore (μm).

As shown in Fig. 12, the PSDs are in good agreement with the SWCCs. The DPSs correspond to the inflection points of boundary stage and transient stage, which are also strikingly related to the AOV and the path length during the transient stage: a larger dominant pore results in a smaller AOV, but in a wider suction range during the transient stage. Since the AOV_1 is not very consistent with the AOV_2 using ULPS value, more researches are needed to assess the start of air occlusion needs to be investigated in the future. In addition, the pore contents of all specimens coincide at $\sim 0.5 \mu\text{m}$ and the suction calculated by the Yang-Laplace equation is $\sim 100 \text{ kPa}$, which is equal to the intersection of the measured SWCCs. Therefore, the intersection of the SWCCs of the five specimens with different dry densities at 100 kPa and their tendency to coincide can be attributed to their almost equal pore distributions in the range of $\leq 0.5 \mu\text{m}$.

As illustrated in Fig. 12, the reviews by Lu and Khorshidi (2015) and Lu (2016) indicated that water in soil can be physically and quantitatively decomposed into two components under the local thermodynamic equilibrium principle at any state of matric suction (Revil et al. 2013): (1) adsorption and; (2) capillarity. This suggests that the compacted specimens with different dry densities have similar adsorption stages due to similar micro-pore distributions. However, the specimens have different capillary stages due to the control of this stage by larger pores.

The high suction stage below the residual value is mainly controlled by adsorption [Fig. 13(a)]. Adsorption is only controlled by the mineral species and quantity and has little relation to the pore diameter distribution (Lu 2016). Therefore, specimens of different dry densities prepared from the same soil should have the same ability to adsorb water mass, with the difference of equal mass only reflects in the pore volume), whereas the mineral types and quantities remain the same. Some studies using isothermal adsorption experiments have suggested that the thickness of the adsorbed water film of loess is 0.36–2 nm. Therefore, the nanometer-level pores should be filled with adsorbed water under the situation of all soil particles being surrounded by adsorbed water.

During the wetting process, the short-range suction effect of soil particles results in the outermost layer of water molecules becoming weaker or even disappearing with a decrease in suction. This results in the water film formed by adsorbed water becoming loose and movable, thereby forming a state of co-dependence between adsorbed water and capillary water [Fig. 13(b)]. Capillarity becomes the sole driver of soil moisture change when adsorbed water reaches its capacity (Lu 2016). The differences in the water holding capacities of soil with different dry densities is mainly reflected in the change in capillary water due to capillarity mainly occurring in inter-granular pores.

Summary And Conclusions

The present study conducted a series of experiments to investigate the SWCCs of compacted loess soil of different dry densities during the wetting process. 2D-SEM images and PSD curves have been used to study the micro-mechanisms of the SWCCs. The main conclusions of the present study are given below:

(1) The SWCCs of compacted loess soil can be characterized by two segments: (i) the lower suction range (0–100 kPa), including boundary stage and transient stage; (ii) the higher suction range (>100 kPa), corresponding to residual stage. The suction of the SWCCs in the lower suction range increases with increasing dry density, whereas that in the higher suction range is almost identical among the five dry density groups. In addition, saturated water content decreases from 34.5% to 18.7% with increasing dry density from 1.40 g/cm⁻³ to 1.80 g/cm⁻³, whereas the AOV increases from 8 kPa to 25 kPa, and the range of the boundary zone increases whereas that of the transient zone decreased.

(2) The pore size distribution directly affects the soil water characteristics. Within the meso-pore range of 1–16 μm, the dominant pore radius and upper limit pore radius decreases with increasing dry density and approaches the lower limit (equal to 2 μm and 3 μm responsibility) as dry density exceeding 1.70 g/cm⁻³.

The pore size distribution within the micro-pore range of less than 0.5 μm remains almost unchanged. Accordingly, the increase in suction with increasing dry density mainly occurs during the capillary stage dominated by meso-pores, whereas suction is identical in the adsorption stage dominated by micro-pores.

(3) The microstructure images indicate features typical of solid particles and pores. Similar particle shapes are evident among the specimens of different dry densities. However, gradual increases occurs in the solid particle area, the contact area, and the aggregate or coagulum number with increasing dry density. Correspondingly, there are decreases in the size and number of pores, resulting in a decrease in the saturated water content.

Declarations

Data Availability

The data used to support the findings of this study are available from the corresponding author upon request.

Conflicts of Interest

The authors declare that there is no conflict of interest regarding the publication of this paper.

Funding Statement

The study was supported by the National Natural Science Foundation of China (Grant No. 41790442, 41772278, 41807242). The above financial supports are gratefully acknowledged.

References

Al-Khafaf S, Hanks RJ (1974) Evaluation of the Filter Paper Method for Estimating Soil Water Potential. *Soil Science* 117(4):194-199. doi:10.1097/00010694-197404000-00003

Altuhafi FN, Coop MR, Georgiannou VN (2016) Effect of particle shape on the mechanical behavior of natural sands. *Journal of Geotechnical and Geoenvironmental Engineering* 142(12):4016071. doi:10.1061/(ASCE)GT.1943-5606.0001569

ASTM. (2011) Standard test method for measurement of soil potential (suction) using filter paper. American Society for Testing and Materials doi D5298

Bharat TV, Gopak Y (2020) Soil water characteristic curves of bentonites in isochoric conditions during wetting: measurement and prediction. *Canadian Geotechnical Journal* (4). doi:10.1139/cgj-2019-0818

Birle E, Heyer D, Vogt N (2008) Influence of the initial water content and dry density on the soil-water retention curve and the shrinkage behavior of a compacted clay. *Acta Geotechnica* 3(3):191-200.

doi:10.1007/s11440-008-0059-y

Baker R, Frydman S (2009) Unsaturated soil mechanics: Critical review of physical foundations. *Engineering Geology* 106(1-2):26-39. doi:10.1016/j.enggeo.2009.02.010

Birle E (2012) Effect of initial water content and dry density on the pore structure and the soil-water retention curve of compacted clay. In *Unsaturated Soils: Research and Applications* (pp.145-152). Springer, Berlin, Heidelberg. doi:10.1007/978-3-642-31116-1_19

Deacon LJ, Grinev DV, Crawford J W, Harris, J., Ritz, K., Young IM (2008) Simultaneous Preservation of Soil Structural Properties and Phospholipid Profiles: A Comparison of Three Drying Techniques. *Pedosphere* 18(3):284-287. doi:10.1016/S1002-0160(08)60018-1

Delage P, Audiguier M, Cui YJ, Howat MD (1996) Microstructure of a compacted silt. *Canadian Geotechnical Journal* 33(1):150-158. doi: 10.1139/t96-030

Delage P (2007) Microstructure features in the behaviour of engineered barriers for nuclear waste disposal. In *Experimental unsaturated soil mechanics* (pp.11-32). Springer, Berlin, Heidelberg. doi:10.1007/3-540-69873-6_2

Della Vecchia G, Jommi C, Romero E (2011) An insight into the water retention properties of compacted clayey soils. *Géotechnique* 61(4):313-328. doi:10.1007/3-540-69873-6_2

Diamond S (1970) Pore size distributions in clays. *Clays and clay minerals* 18(1):7-23. doi:10.1346/CCMN.1970.0180103

Eyo E, Ngambi S, Abbey SJ (2020) An overview of soil-water characteristic curves of stabilised soils and their influential factors. *Journal of King Saud University Science* doi:10.1016/j.jksues.2020.07.013

Fredlund, Delwyn G (2006) Unsaturated soil mechanics in engineering practice. *Journal of Geotechnical and Geoenvironmental Engineering* 132(3):286-321. doi:10.1061/(ASCE)1090-0241(2006)132:3(286

Gao Guorui, Gao Guoyou (1980) Microstructures of loess soil in China. *A Monthly Journal of Science* (07):63-67. (in Chinese) CNKI:SUN:JAXG.0.1981-07-007

Gao Guorui (1981) Classification of microstructure of loess in China and their collapsibility. *Scientia Sinica Ser.A*(07):962-974. (in Chinese) CNKI:SUN:JXTW.0.1980-07-013

International A (2006) Standard practice for classification of soils for engineering purposes (Unified Soil Classification System). Astm

Jiang M, Zhang F, Hu H, Cui Y, Peng J (2014) Structural characterization of natural loess and remolded loess under triaxial tests. *Engineering Geology* 181:249-260. doi:10.1016/j.enggeo.2014.07.021

Jiang M (2019) New paradigm for modern soil mechanics: Geomechanics from micro to macro.

Chinese Journal of Geotechnical Engineering 41.02(2019):195-254. (in Chinese) CNKI:SUN:YTGC.0.2019-02-002

Jiang Y, Chen W, Wang G, Sun G, Zhang F (2017) Influence of initial dry density and water content on the soil-water characteristic curve and suction stress of a reconstituted loess soil. *Bulletin of Engineering Geology and the Environment* 76(3):1085-1095. doi:10.1007/s10064-016-0899-x

Hou X, Qi S, Li T, Guo S, Wang Y, Li Y, Zhang L (2020) Microstructure and soil-water retention behavior of compacted and intact silt loess. *Engineering Geology* 277:105814. doi:10.1016/j.enggeo.2020.105814

Kim H, Tang D, Ganju E, Prezzi M, Salgado R (2019) Experimental investigation of matric suction in compacted fine-grained soils. *International Journal of Pavement Engineering* 20(1):53-60. doi:10.1080/10298436.2016.1258242

Li H, Li TL, Li P, Zhang YG (2020) Prediction of loess soil-water characteristic curve by mercury intrusion porosimetry. *Journal of Mountain Science* 17(9):2203-2213. doi:10.1007/s11629-019-5929-2

Li H, Li T, Jiang R, Wang Y, Zhang Y (2020) A new method to simultaneously measure the soil–water characteristic curve and hydraulic conductivity function using filter paper. *Geotechnical Testing Journal* 43(6):20190162. doi:10.1520/GTJ20190162

Li P, Li T, Vanapalli SK (2018) Prediction of soil-water characteristic curve for Malan loess in Loess Plateau of China. *Journal of Central South University* 25(2):432-447. doi: 10.1007/s11771-018-3748-1.

Li X, Li L (2017) Quantification of the pore structures of Malan loess and the effects on loess permeability and environmental significance, Shaanxi Province, China: an experimental study. *Environmental Earth Sciences* 76(15):1-14. doi:10.1007/s12665-017-6855-7.

Li X, Li L, Song Y, Hong B, Wang L, Sun J (2019) Characterization of the mechanisms underlying loess collapsibility for land-creation project in Shaanxi Province, China—a study from a micro perspective. *Engineering Geology* 249: 77-88. doi:10.1016/j.enggeo.2018.12.024

Li P, Qian H, Wu J (2014) Environment: Accelerate research on land creation. *Nature* 510(7503):29-31. doi:10.1038/510029a

Li Y (2013) Effects of particle shape and size distribution on the shear strength behavior of composite soils. *Bulletin of engineering geology and the environment* 72(3-4):371-381. doi: 10.1007/s10064-013-0482-7.

Lu N, Likos WJ (2006) Suction stress characteristic curve for unsaturated soil. *Journal of Geotechnical and Geoenvironmental Engineering* 132(2):131-142. doi:10.1061/(ASCE)1090-0241(2006)132:2(131).

Lu N, Khorshidi M (2015) Mechanisms for soil-water retention and hysteresis at high suction range. *Journal of Geotechnical and Geoenvironmental Engineering* 141(8):04015032.

doi:10.1061/(ASCE)GT.1943-5606.0001325

Lu N (2016) Generalized soil water retention equation for adsorption and capillarity. *Journal of Geotechnical and Geoenvironmental Engineering* 142(10):04016051. doi:10.1061/(ASCE)GT.1943-5606.0001524

Lu N (2019) Linking soil water adsorption to geotechnical engineering properties. In *Geotechnical Fundamentals for Addressing New World Challenges* (pp.93-139). Springer, Cham. doi:10.1007/978-3-030-06249-1_4

Mbonimpa M, Aubertin M, Maqsoud A, Bussière B (2006) Predictive model for the water retention curve of deformable clayey soils. *Journal of Geotechnical and Geoenvironmental Engineering* 132(9):1121-1132. doi:10.1061/(ASCE)1090-0241(2006)132:9(1121).

Miguel MG, Bonder BH (2012) Soil-water characteristic curves obtained for a colluvial and lateritic soil profile considering the macro and micro porosity. *Geotechnical and Geological Engineering* 30(6):1405-1420. doi:10.1007/s10706-012-9545-y

Mijares RG, Khire MV (2010) Soil water characteristic curves of compacted clay subjected to multiple wetting and drying cycles. *Geotechnical Special Publication* (199):400-409. doi:10.1061/41095(365)37

Nie B, Liu X, Yang L, Meng J, Li X (2015) Pore structure characterization of different rank coals using gas adsorption and scanning electron microscopy. *Fuel* 158(oct.15):908-917. doi:10.1016/j.fuel.2015.06.050

Ning L, Likos WJ (2004) *Unsaturated soil mechanics*. J. Wiley. ISBN: 9780471447313

Pagliai M, Vignozzi N, Pellegrini S (2004) Soil structure and the effect of management practices. *Soil and Tillage Research* 79(2):131-143. doi:10.1016/j.still.2004.07.002

Pincus HJ, Houston SL, Houston WN, Wagner AM (1994) Laboratory Filter Paper Suction Measurements. *Geotechnical Testing Journal* 17(2):185-194. doi:10.1520/GTJ10090J

Rahardjo H, Leong EC (2006) Suction measurements. *Unsaturated Soils* (pp.81-104). doi:10.1061/40802(189)3

Ran H, Chen Y, Liu H, Zhou C (2013) A water retention curve and unsaturated hydraulic conductivity model for deformable soils: Consideration of the change in pore-size distribution. *Géotechnique* 63(16):1389-1405. doi:10.1680/geot.12.P182

Revil A, Lu N (2013) Unified water isotherms for clayey porous materials. *Water Resources Research* 49(9):5685-5699. doi:10.1002/wrcr.20426

Romero E, Gens A, Lloret A (1999) Water permeability, water retention and microstructure of unsaturated compacted Boom clay. *Engineering Geology* 54(1-2):117-127. doi:10.1016/S0013-7952(99)00067-8

- Sasanian S, Newson TA (2013) Use of mercury intrusion porosimetry for microstructural investigation of reconstituted clays at high water contents. *Engineering Geology* 158:15-22.
doi:10.1016/j.enggeo.2013.03.002
- Salager S, Nuth M, Ferrari A, Laloui L (2013) Investigation into water retention behaviour of deformable soils. *Canadian Geotechnical Journal* 50(2):200-208. doi:10.1139/cgj-2011-0409
- V. Genuchten, M. Th (1980) A closed-form equation for predicting the hydraulic conductivity of unsaturated soils. *Soil Science Society of America Journal* 44(5): 892-898.
doi:10.2136/sssaj1980.03615995004400050002x
- Vanapalli SK, Fredlund DG, Pufahl DE (2001) Influence of soil structure and stress history on the soil-water characteristics of a compacted till. *Géotechnique* 51(6):573-576. doi:10.1680/geot.51.6.573.40456
- Washburn EW (1921) Note on a method of determining the distribution of pore sizes in a porous material. *Proceedings of the National Academy of Sciences of the United States of America* 7(4):115-116.
doi:10.1073/pnas.7.4.115
- Wang JD, Li P, Ma Y, Vanapalli SK, Wang XG (2019) Change in pore-size distribution of collapsible loess due to loading and inundating. *Acta Geotechnica* 15(5):1081-1094 doi:10.1007/s11440-019-00815-9
- Xu P, Zhang Q, Qian H, Qu W, Li M (2020) Microstructure and permeability evolution of remolded loess with different dry densities under saturated permeation. *Engineering Geology* 282(7):105875.
doi:10.1016/j.enggeo.2020.105875
- Yang X, Wang J, Zhu C, He M, Gao Y (2019) Effect of wetting and drying cycles on microstructure of rock based on SEM. *Environmental Earth Sciences* 78(6):1-10. doi:10.1007/s12665-019-8191-6
- Zhang P, Fang YG, Yan XQ, He ZW (2011) Study of different dry methods for drying remolded bentonite sample with mercury intrusion test. *Rock and Soil Mechanics* 32:388-391. (in Chinese)
doi:CNKI:SUN:YTLX.0.2011-S1-070
- Zhang X, Mavroulidou M, Gunn MJ (2017) A study of the water retention curve of lime-treated London Clay. *Acta Geotechnica* 12(1):23-45. doi:10.1007/s11440-015-0432-6
- Zhou AN, Sheng D, Carter JP (2012) Modelling the effect of initial density on soil-water characteristic curves. *Geotechnique* 62(8):669-680. doi:10.1680/geot.10.P120

Tables

Table 1. Physical parameters of the compacted specimens prepared from soil taken from the land preparation area of Yan'an City, China

Specimen number	No. 1	No. 2	No. 3	No. 4	No. 5
Dry density (g cm ⁻³)	1.40	1.50	1.60	1.70	1.80
Void ratio	0.936	0.807	0.694	0.594	0.506
Degree of compaction	0.78	0.83	0.89	0.94	1
Parameters	Molding water content	Specific gravity	Plastic limit	Liquid limit	Plasticity index
Same value	10%	2.71	18.7	18.8	9.8

Table 2. The fitting parameters of the Van Genuchten (1980) model applied to five specimens

Specimen number	No. 1	No. 2	No. 3	No. 4	No. 5
Dry density (g cm ⁻³)	<u>1.4</u>	<u>1.5</u>	<u>1.6</u>	<u>1.7</u>	<u>1.8</u>
<i>a</i>	<u>0.043</u>	<u>0.035</u>	0.030	<u>0.023</u>	<u>0.019</u>
<i>n</i>	<u>2.083</u>	<u>2.526</u>	2.473	<u>3.194</u>	<u>3.194</u>
<i>m</i>	<u>0.986</u>	<u>0.984</u>	0.991	<u>1.001</u>	<u>1.009</u>
<i>R</i> ²	<u>0.955</u>	<u>0.989</u>	0.991	<u>0.980</u>	<u>0.972</u>
<i>w</i> _s	<u>34.5%</u>	<u>29.8%</u>	<u>25.6%</u>	<u>21.9%</u>	<u>18.7%</u>
AOV (kPa)	8	<u>11</u>	<u>13</u>	<u>22</u>	<u>25</u>
RV (kPa)	<u>100</u>	<u>100</u>	<u>100</u>	<u>100</u>	<u>100</u>

Figures

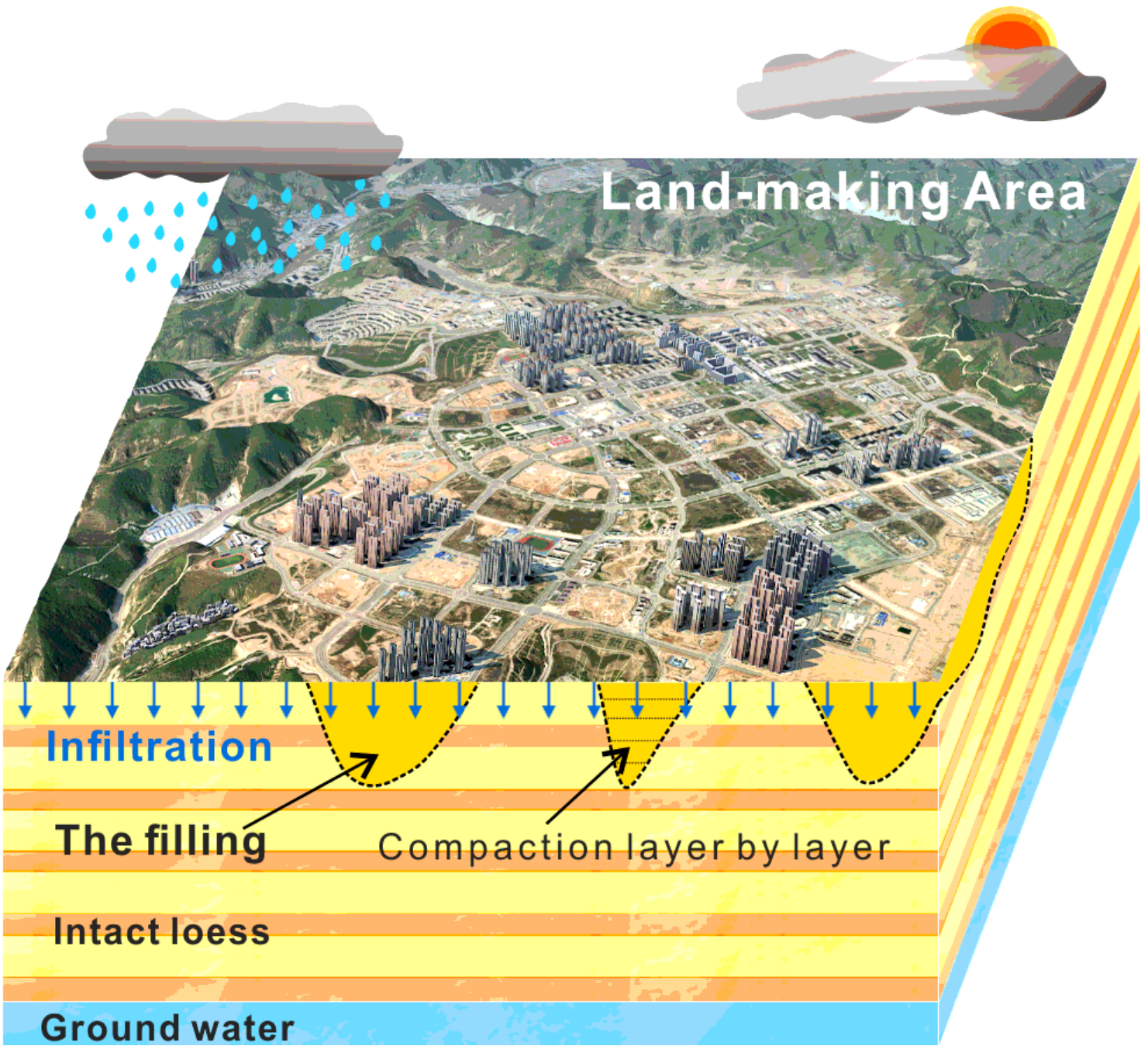


Figure 1

The filled loess in the new district of the city of Yan'an, China

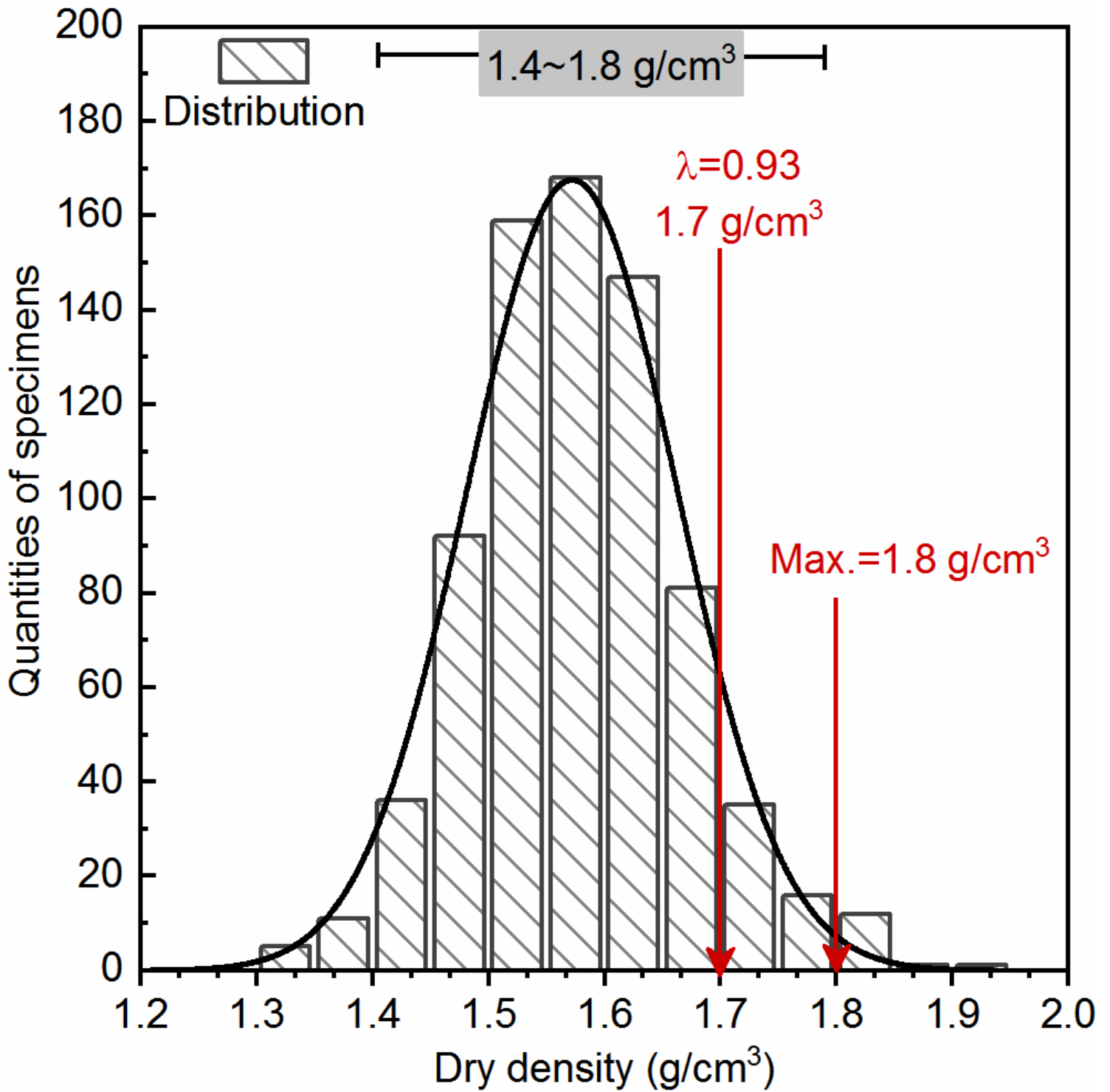


Figure 2

The results of laboratory tests of 19 boreholes in the filled soil area indicate a normal distribution of the dry densities of the compacted loess specimens, mostly in the range of 1.40–1.80 g/cm⁻³, accounting for 97% of the total.

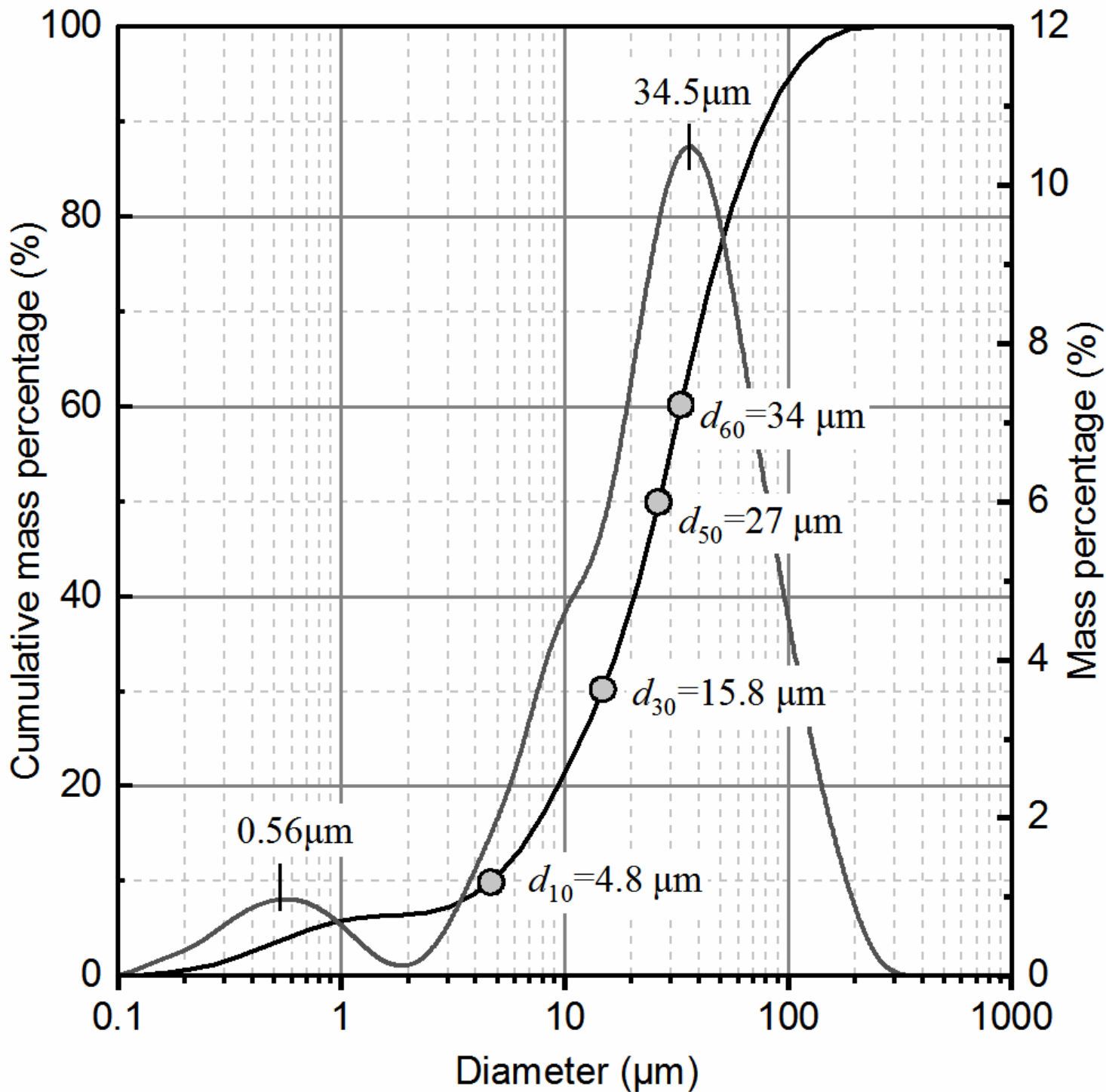


Figure 3

The particle size distribution of the soil was analyzed using the Battersize-2000 Laser Analyzer. Silt (0.002–0.05 mm) and clay (< 0.002 mm) particles comprised 65.96% and 6.55% of the total soil particles, respectively.

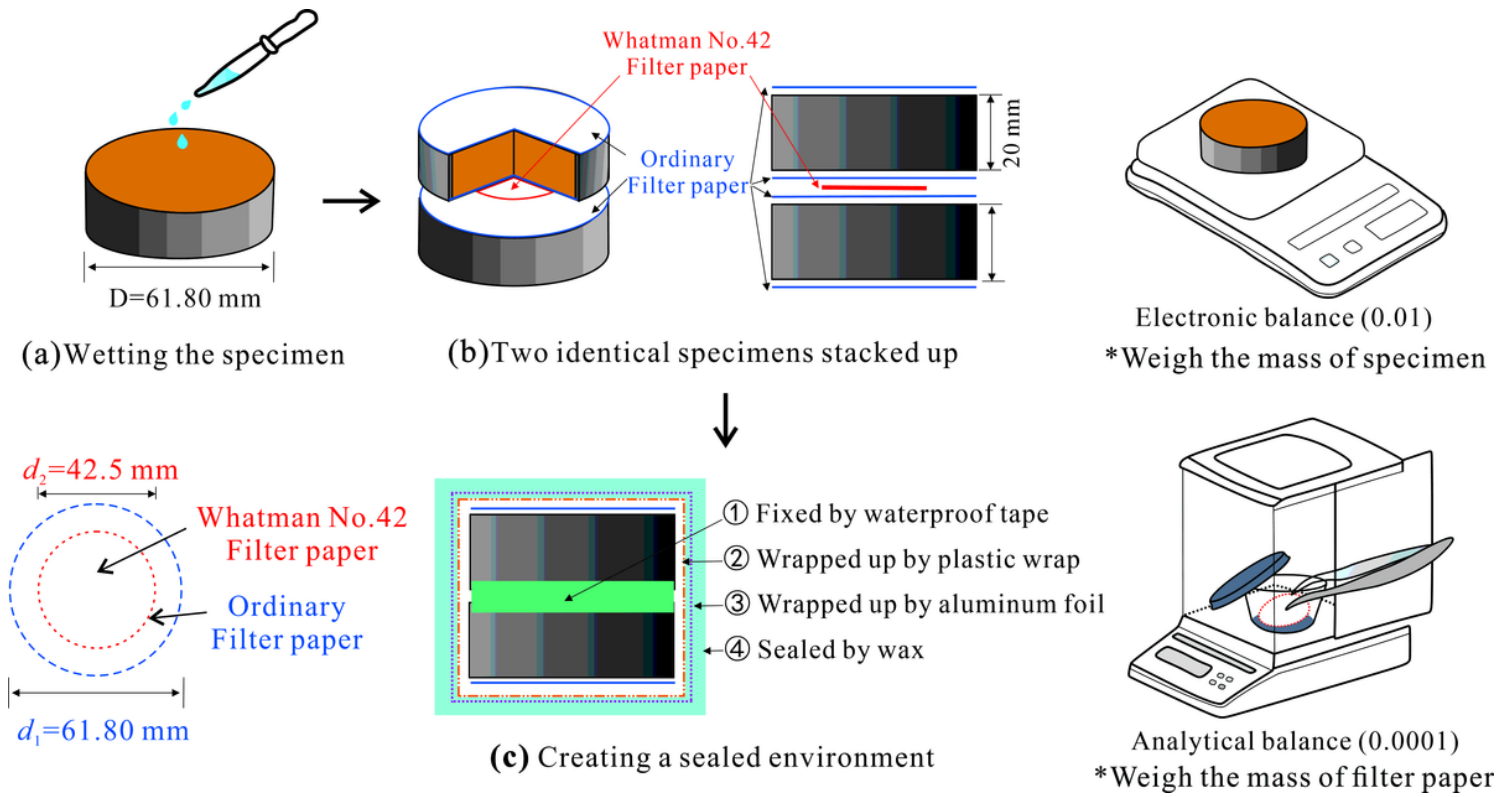


Figure 4

SWCC of the compacted specimens was measured by FPM,

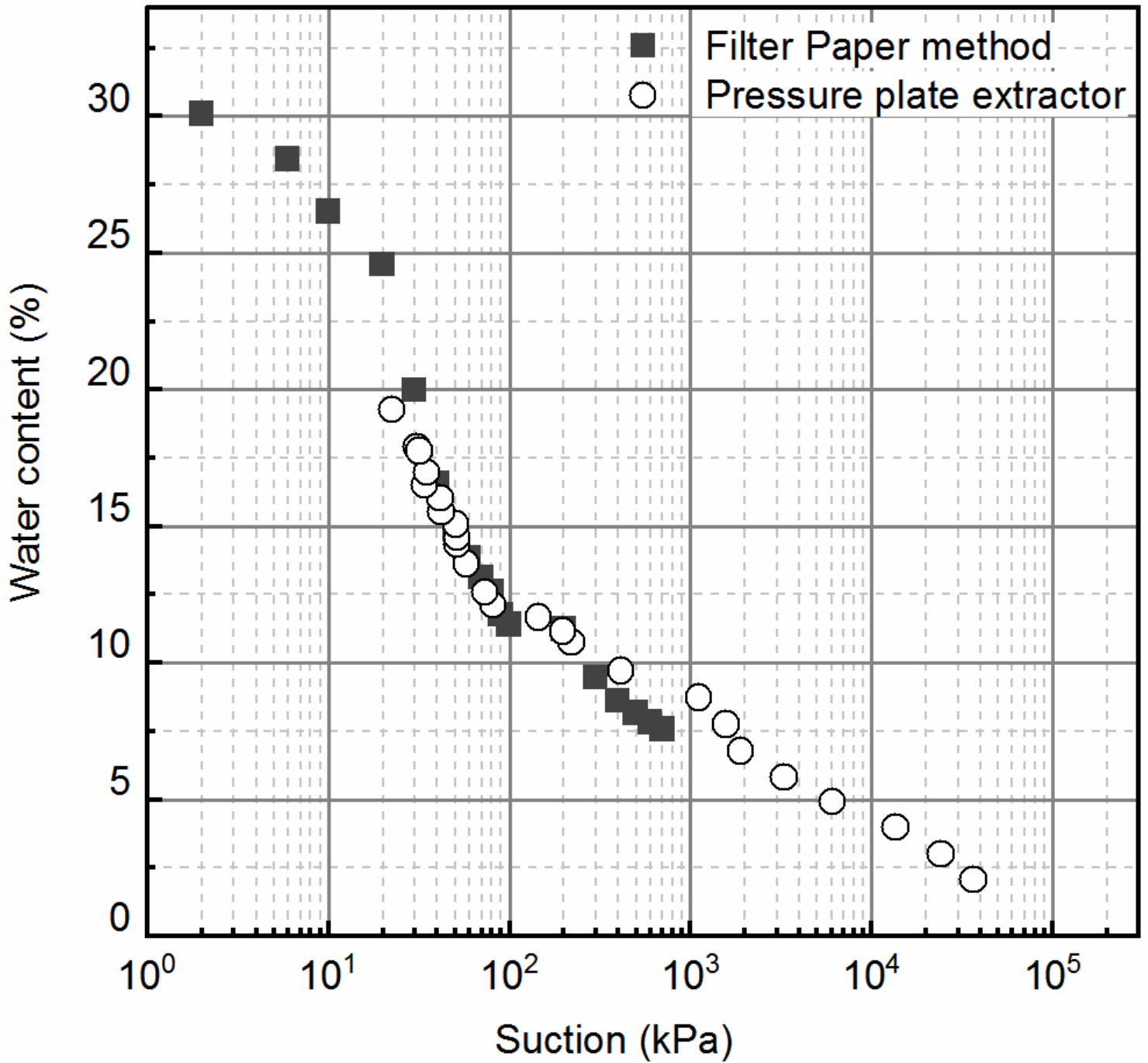


Figure 5

Soil water content against matric suction of the No.2 specimen (hollow circles). The experimental results of the pressure plate method are also plotted in Fig. 5 (black squares) in the lower suction range, which indicates a good agreement between the data of the two methods in the overlap range.

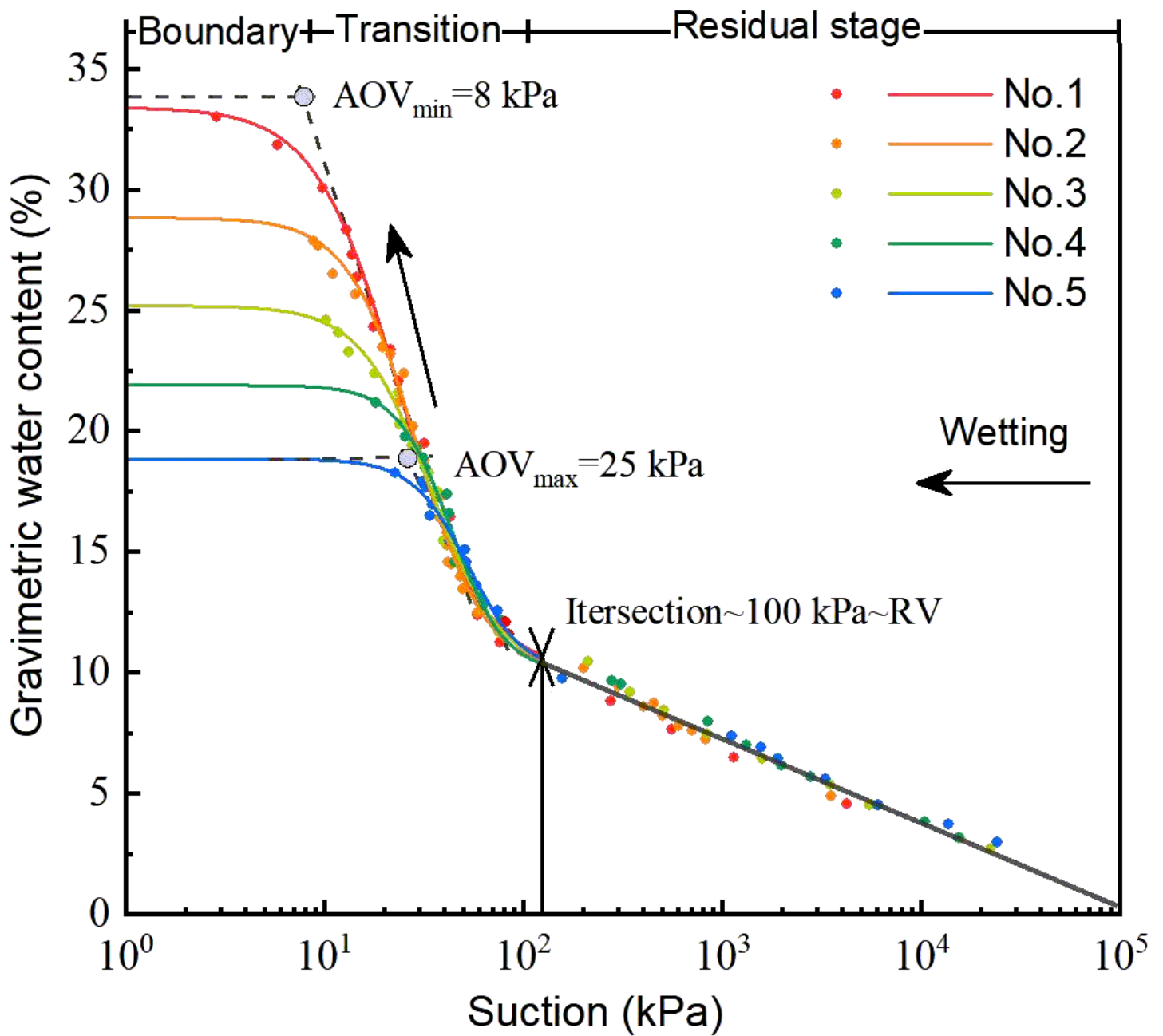


Figure 6

The SWCCs can be divided into three stages (Vanapalli et al. 1999): (1) the boundary effect stage; (2) the transient stage and; (3) the residual stage.

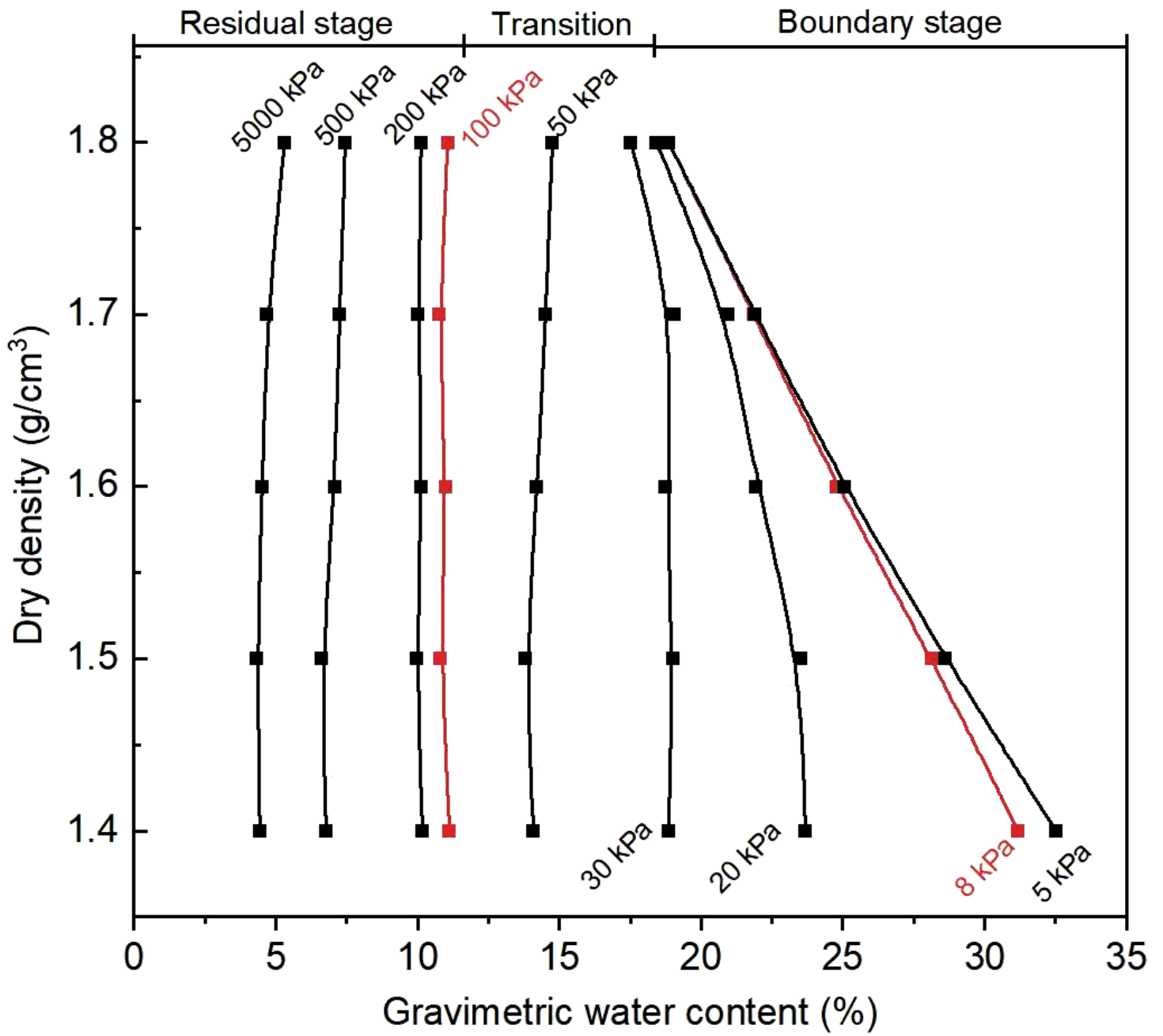


Figure 7

The equi-suction lines in Fig. 7 shows that lines for suction below 100 kPa have a varied degree of inclination.

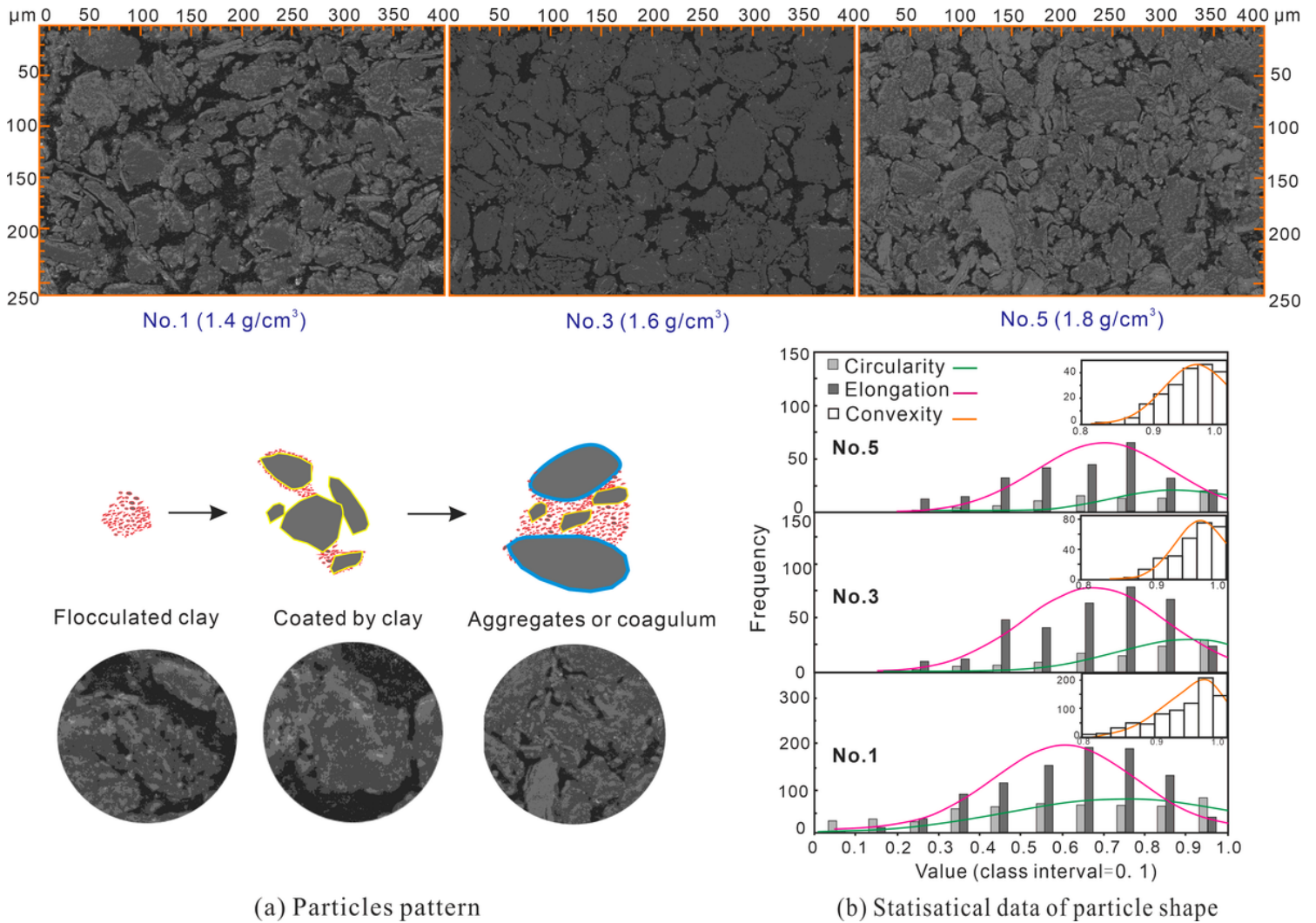


Figure 8

(a) shows 2D images of the soil specimens with dry densities of 1.40 g/cm⁻³ (No. 1), 1.60 g/cm⁻³ (No. 3), and 1.80 g/cm⁻³ (No. 5) captured using SEM at a magnification of $\times 1,000$. The compacted soil is an assemblage of particles and aggregations (Della et al. 2011), and the particles can be subdivided into sand ($> 60 \mu\text{m}$), silt ($2-60 \mu\text{m}$), and clay ($< 2 \mu\text{m}$). Within the captured 2D-SEM images at $\times 1,000$ magnification, clay particles have a radius of less than $1 \mu\text{m}$ and are hard to identify, whereas silt and sand particles can be clearly observed. It can be seen from Fig. 8(a) that for specimens with the same soil properties and molding water content, the total area of particles increases with increasing dry density, the contact between particles changes from point-to-point contact to surface contact, and the number of aggregates or coagulum gradually increases. The results of the present study indicate no obvious concentrated distribution in the circularity of particles in each specimen, with elongation in the range of 0.5–0.8 and convexity mostly exceeding 0.90 [Fig. 8 (b)]

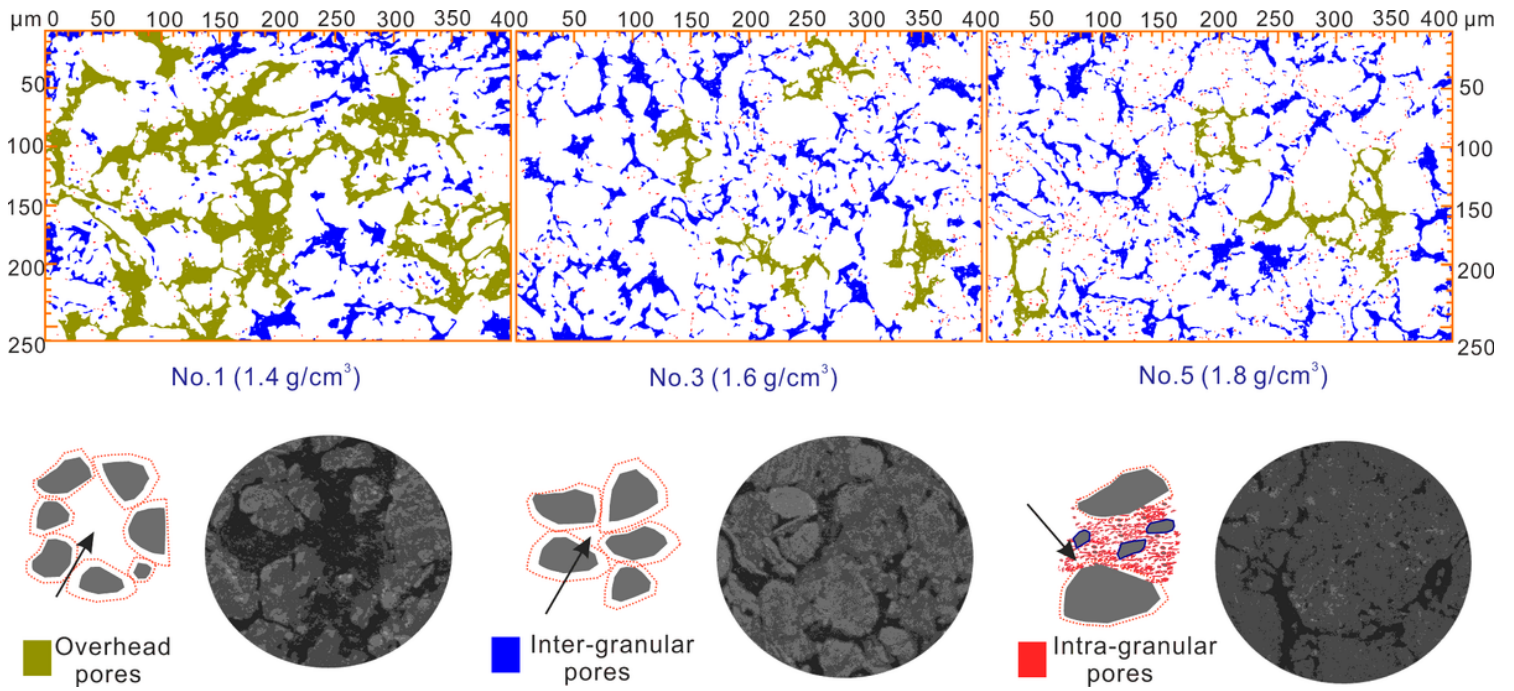


Figure 9

The processing of 2D-SEM images by IPP 6.0 allows the pore elements to be separately identified and rendered. an increase in dry density results in a reduction of overhead pores (green area) and an increase in inter-granular pores (blue area). There is no comparison and discussion on micropores since they cannot be accurately identified in the current study.

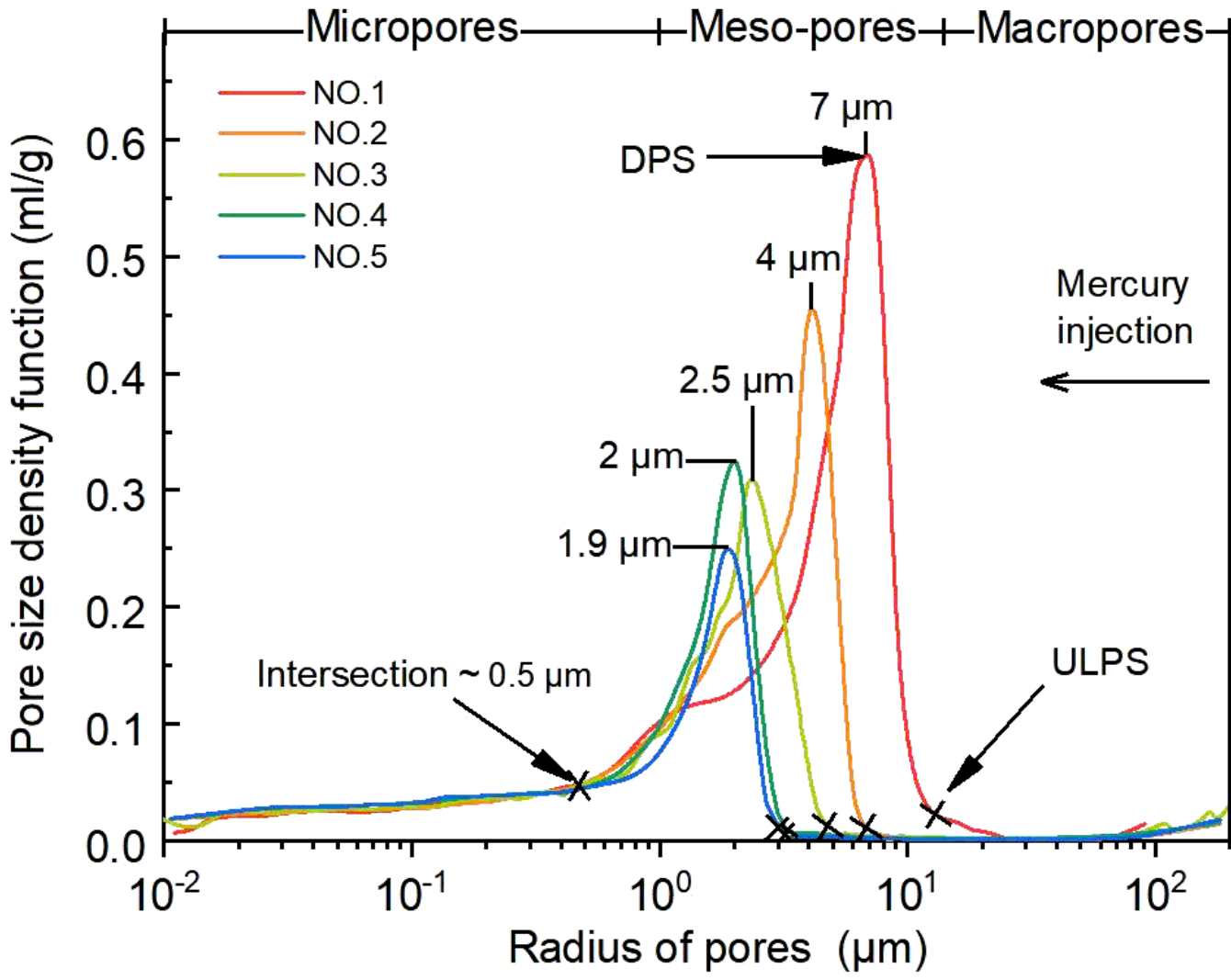


Figure 10

The pore size distribution (PSD) curves of the five specimens are measured by MIP to quantitatively investigate the pore characteristics of specimens with different dry densities

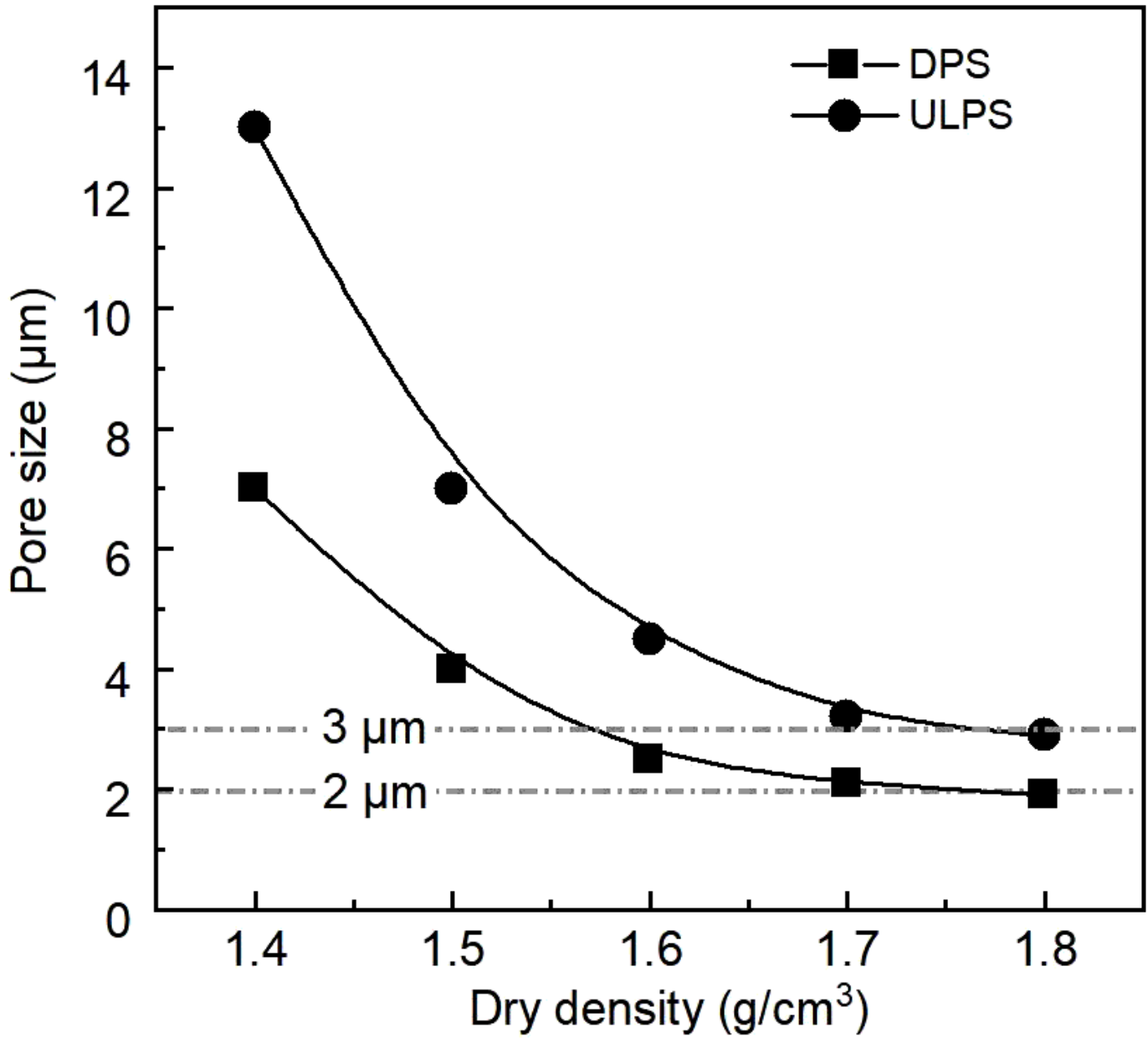


Figure 11

The differences in DPS and ULPS decrease rapidly and tend to stabilize. Both the DPS and ULPS of No. 1 are the largest, whereas those of No. 4 and No. 5 are the smallest.

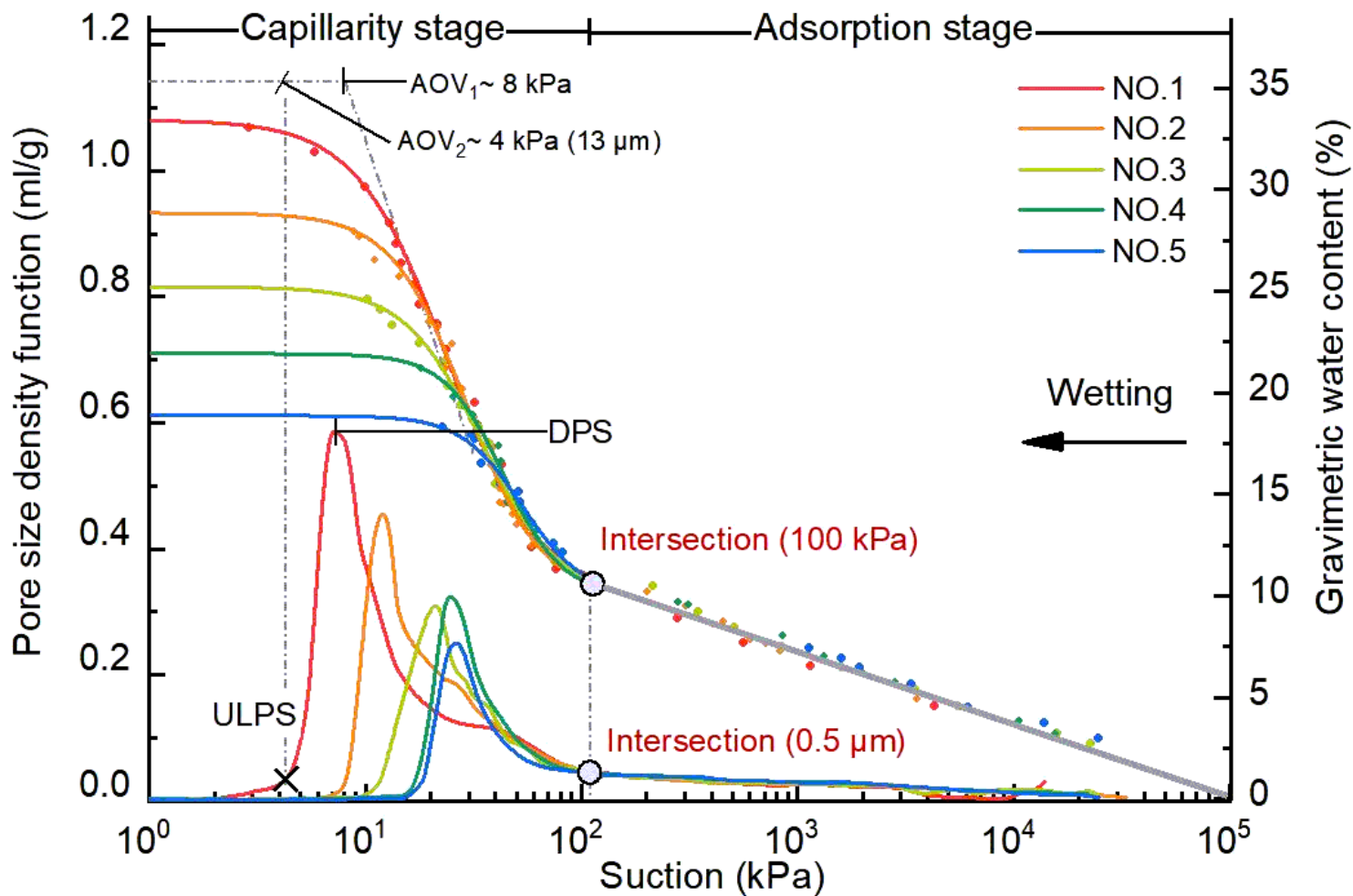


Figure 12

The PSDs are in good agreement with the SWCCs.

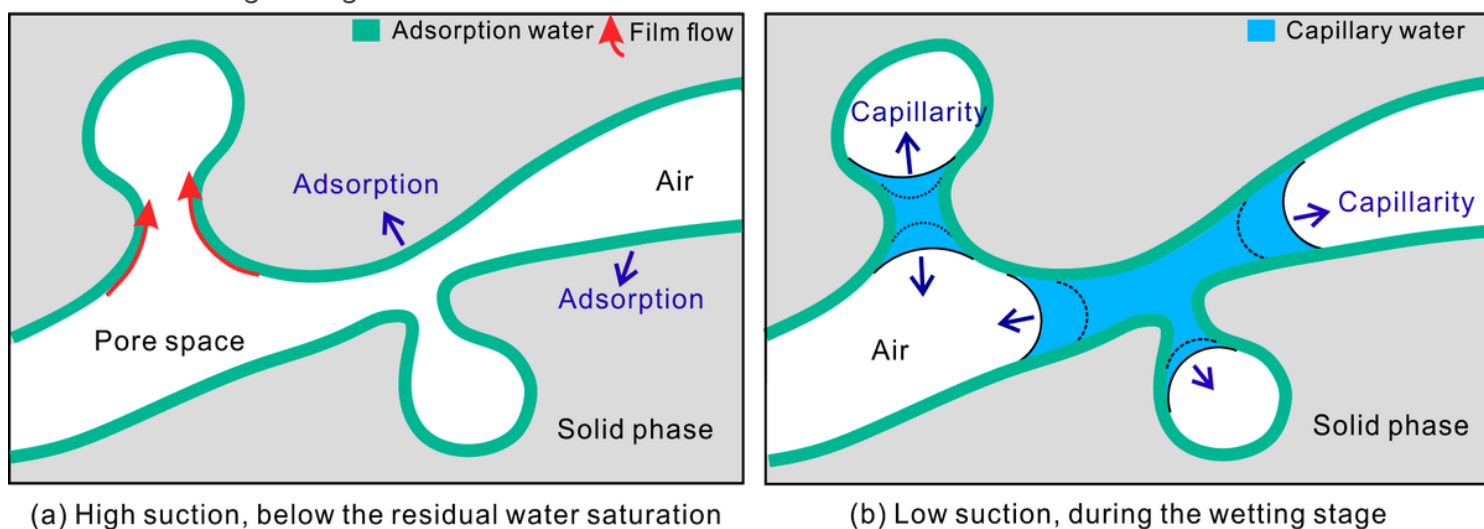


Figure 13

The high suction stage below the residual value is mainly controlled by adsorption [Fig. 13(a)]. The water film formed by adsorbed water becoming loose and movable, thereby forming a state of co-dependence between adsorbed water and capillary water [Fig. 13(b)].